INTERFACE FOCUS

rsfs.royalsocietypublishing.org

Research

Cite this article: Bokka KK, Jesudason EC, Warburton D, Lubkin SR. 2016 Quantifying cellular and subcellular stretches in embryonic lung epithelia under peristalsis: where to look for mechanosensing. *Interface Focus* **6**: 20160031.
http://dx.doi.org/10.1098/rsfs.2016.0031

One contribution of 12 to a theme issue 'Coupling geometric partial differential equations with physics for cell morphology, motility and pattern formation'.

Subject Areas:
biomechanics, biomathematics

Keywords:
lung, airway, peristalsis, deformation, stenosis, morphogenesis

Author for correspondence:
Sharon R. Lubkin
e-mail: lubkin@ncsu.edu

Quantifying cellular and subcellular stretches in embryonic lung epithelia under peristalsis: where to look for mechanosensing

Kishore K. Bokka[1], Edwin C. Jesudason[2], David Warburton[3] and Sharon R. Lubkin[1]

[1]North Carolina State University, Raleigh, NC 27695, USA
[2]Paediatric Surgery, University of Liverpool, Liverpool L69 3BX, UK
[3]Saban Research Institute, 4650 Sunset Boulevard, MS# 35, Los Angeles, CA 90027, USA

SRL, 0000-0003-2521-0699

Peristalsis begins in the lung as soon as the smooth muscle (SM) forms, and persists until birth. As the prenatal lung is filled with liquid, SM action can, through lumen pressure, deform tissues far from the immediately adjacent tissues. Stretching of embryonic tissues has been shown to have potent morphogenetic effects. We hypothesize that these effects are at work in lung morphogenesis. In order to refine that broad hypothesis in a quantitative framework, we geometrically analyse cell shapes in an epithelial tissue, and individual cell deformations resulting from peristaltic waves that completely occlude the airway. Typical distortions can be very large, with opposite orientations in the stalk and tip regions. Apical distortions are always greater than basal distortions. We give a quantitative estimate of the relationship between length of occluded airway and the resulting tissue stretch in the distal tip. We refine our analysis of cell stresses and strains from peristalsis with a simple mechanical model of deformation of cells within an epithelium, which accounts for basic subcellular geometry and material properties. The model identifies likely stress concentrations near the nucleus and at the apical cell–cell junction. The surprisingly large strains of airway peristalsis may serve to rearrange cells and stimulate other mechanosensitive processes by repeatedly aligning cytoskeletal components and/or breaking and reforming lateral cell–cell adhesions. Stress concentrations between nuclei of adjacent cells may serve as a mechanical control mechanism guiding the alignment of nuclei as an epithelium matures.

1. Introduction

Peristalsis is a widespread transport mechanism, operating in systems from digestive to vascular to secretory to excretory. It is an ancient phenomenon, present in metazoa even as simple as cnidarians, and is hypothesized to have originated more than 600 Ma [1]. There are decades of research aimed at understanding the functioning of peristaltic transport by studying the fluid–structure interactions. Until recent computational advances permitted a wider range of models, analysis of peristalsis was done using simplified models, such as small-amplitude two-dimensional channel flow, which could be analysed with pencil and paper. These simple models yielded a rich understanding of the fluid mechanics. Peristalsis has more realistically been modelled as in an infinitely long tube, where it exhibits richly varied behaviours [2–8]. For example, although it may be initially counterintuitive, a peristaltic wave moving to the right creates reflux (counterflow) to the left [3,4]. Other models have explained the phenomenon known as 'trapping', in which a toroidally rolling bolus of fluid moves with the peristaltic wave [3,9]. Advances

THE ROYAL SOCIETY PUBLISHING

in computation in recent decades have permitted the simulation of more complex or challenging peristaltic models (e.g. [10]). The physics and engineering of *open-ended* peristalsis are thus by now well understood. Consequently, peristaltic pumping is not just an important natural transport mechanism, but also is widespread in industrial and medical use. However, until recently [11,12], there has not been any study of the mechanics of *blind-ended peristalsis*, let alone an understanding of its biological implications.

Airway peristalsis (AP) produces spontaneous phasic airway contractions and transient, reversible airway occlusions throughout normal lung development [13–16]. AP begins as soon as the smooth muscle (SM) develops, concurrently with pseudo-glandular branching, and becomes more robust towards later stages of development.

Mechanical forces have widespread and potent influences on morphogenesis, through a variety of sophisticated mechanisms, at subcellular, cellular, multicellular and long-distance scales, by generation and sensing of tension and compression in tissues, and by generation and sensing of fluid flows (extensively reviewed in [17]). Lung morphogenesis is no exception (reviewed in [18,19]): it is regulated by such diverse mechanical inputs as secretion [20], fetal breathing movements [20], tonic contractions [21] and peristalsis [22].

Although AP has been shown to influence lung development (reviewed in [22]), the mechanisms remain unclear, in part because treatments which reduce AP reduce branching, but the converse also holds: treatments that reduce branching also reduce AP [14]. In order to help disentangle these confounded phenomena, it would help to establish a mechanical basis for the interactions between AP and morphogenesis. Existing *in vitro* studies may not be relevant to a specific mechanical stimulus *in vivo*. 'When applying mechanical deformation to cells *in vitro*, it is very important to choose proper amplitude of cellular deformation to simulate different respiratory maneuvers' [18]. It is also important to choose proper orientation and timing. Establishing a rational geometric and mechanical basis for understanding AP will thus be crucial in designing and interpreting experiments.

In this paper, we examine the hypothesis [22] that AP critically modulates physical forces on airway cells, hence the patterning of branching morphogenesis and, ultimately, the overall growth of the lung [23,24]. That verbal hypothesis is broad and does not specify the location, direction, timing, magnitude or control of those physical forces, all of which would have specific biological implications. Thus, it is worth making the effort to make that broad verbal hypothesis more specific, detailed and quantitative. In many experimental systems, it is not possible to perform an adequately controlled experiment to cleanly distinguish between hypotheses, but in a mathematical model, it is possible to construct a quantitative framework which can not only distinguish between confounded factors, but in some cases rule out some hypothesized mechanisms. For example, in a similar system, the occluded static embryonic lung, we began with a broad mechanical hypothesis [25] and constructed a suite of models examining more specific quantitative aspects of the mechanics, and identifying locations and directions of the relevant tissue stresses and stretches [26]. In that case, our models showed that for stretch reception to be driving enhanced branching in the static occluded lung, there must be non-uniform tissue stiffness or non-uniform mechanoreception, because the location of maximum stresses is not where the branching occurs.

In two recent papers [11,12], we analysed the dynamics of the fluid–structure interactions in the partially occluded embryonic lung undergoing peristalsis. Peristalsis is very different in the cases of *partial occlusion* (PO) and *complete occlusion* (CO). For PO, tissue deformations are relatively small away from the immediate vicinity of the contraction [12], but the flow can be substantial, dramatically increasing mixing and longitudinal transport of lumen contents, which may have a morphogenetic effect [11]. For CO, the flow is negligible but the tissue deformations can be very large, due to the fluid trapped distal to the pinch, and the increase in pressure. In PO, where flow is substantial, there may be flow sensing by primary cilia; we predicted that such flow-sensing cilia would not be found distal to SM, where flow is negligible, and that flow-sensing cilia would be longer near the end of the SM, where flow velocities are small [11]. But mechanosensing could also be from tissue stretch, which is small in PO.

In order to refine the verbal stretch-reception hypothesis in the peristaltic context by more specifically determining the physical forces and substantial tissue distortions of CO, in this paper, we develop and analyse geometric and mechanical models of completely occluded peristalsis in the embryonic airway, and estimate the relationships between tissue geometry, cell geometry, tissue stretch, cell stretch and subcellular stretch and stress.

2. Modelling assumptions

2.1. Airway geometry and histology

In order to focus on the most fundamental aspects of embryonic AP, we model the embryonic lung as a radially symmetric tube with a liquid-filled lumen (figure 1). We neglect tissues other than the epithelium and focus our attention on the relationship between overall constriction of the tubule causing occlusion of the lumen and the resulting deformation of the epithelium. This idealized unbranched shape corresponds to the beginning of the pseudo-glandular period, the period of branching. The simplified geometry and histology also models the immediate vicinity of a distal tip of a later branched embryonic stage. Thus the same model, using different parameters describing tissue stiffness, size, etc. can model two morphogenetic stages.

For geometric analysis, we modelled the relaxed airway epithelial geometry as an unbranched cylindrical tube of uniform thickness, with a hemispherical tip of the same inner and outer radii as the stalk (figure 1*b*). While there are well-established methods for measuring microelasticity of tissues, and tissue stiffness is coupled to nuclear viscoelasticity [27], quantifying or even defining single-cell stiffness within a tissue is problematic for a variety of reasons including internal heterogeneity, complex dynamic response and the observation that cells within a tissue are different from isolated cells. However, a great deal of insight can be gained from a simple model. Therefore, tissue was modelled as having uniform linear elastic isotropic material properties, so that distortions of the tissue exactly determine distortions of the cells. We assumed that, on the timescale of AP, growth and swelling can be neglected, i.e. cell and tissue volume remain constant.

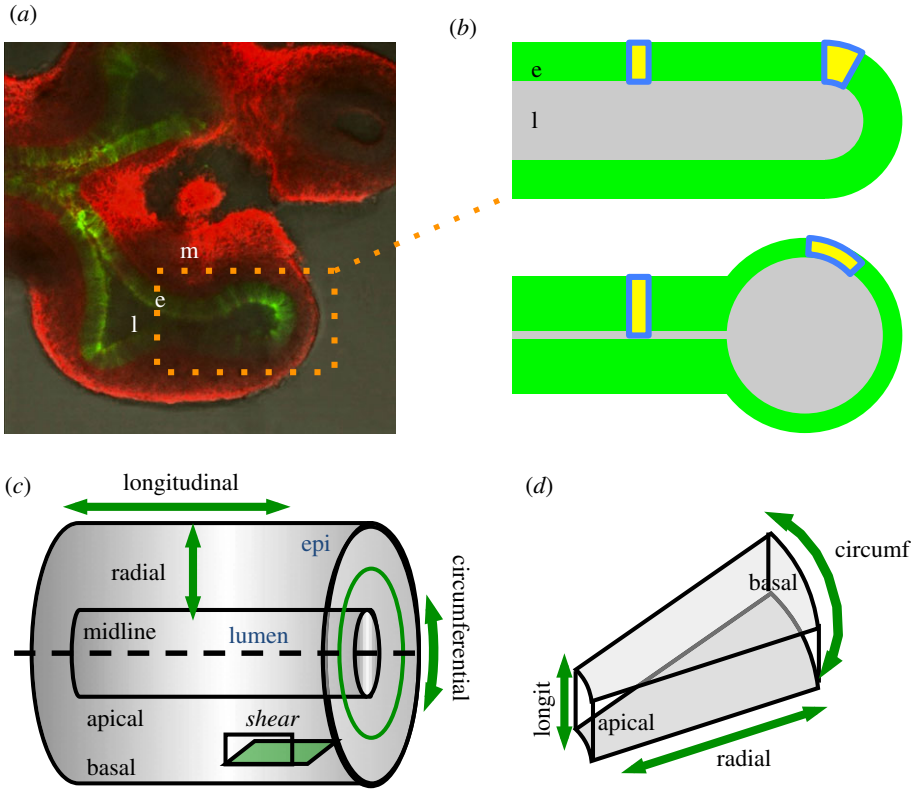

Figure 1. Geometry of embryonic lung and model. (*a*) Explanted E11.5 mouse lung showing lumen (l), epithelium (e, green) and mesenchyme (m, red). Smooth muscle not visible. Peristaltic waves move proximodistally, constricting the stalk while inflating the tips. (*b*) Embryonic lung idealized as unbranched simple epithelial tubule (e), with lumen (l). Approximating stalk as cylinder and tip as sphere or hemisphere allows analytical approximations of the mechanics and geometric distortions of peristalsis. Individual cells (yellow) are deformed the same as the local tissue. (*c*) Orientation in a tubule. Tissue can be stretched or compressed in radial, circumferential, and/or longitudinal directions, and can be sheared in radial–longitudinal interaction. (*d*) Geometry of idealized epithelial cell from stalk region of a tubule.

2.2. Peristaltic distortions of tissue morphology

In our models, peristalsis consists of a wave of contraction propagating from trachea to tip. In contrast with our previous models of PO [11,12], we assume that occlusion is CO, and lumen fluid does not leak, so lumen volume is conserved. We estimate the deformations of individual cells in the epithelium with a simple, purely geometric model, by accounting for conservation of lumen volume and cell volume. Deformation analysis neglects changes in tubule length, which are small relative to radial and circumferential strains. The apical epithelial surface is distorted far more by CO than by PO (as studied in [11,12]). In CO, apical surfaces come into contact, but it is unknown whether, in cross-section, CO is symmetric, like a sphincter, asymmetrically ovaled, like a pinched hose, or gathered into folds. In this paper, for simplicity and in the absence of evidence to the contrary, we model CO of the epithelial tubule as compression of the apical surface's cross-section to a single point, without buckling.

2.3. Cell packing, shape and size

The epithelium is modelled as one cell thick, with uniform cell shapes and uniform packing everywhere in the stalk, and everywhere in the tip. Tip cells are modelled as truncated cones. Stalk cells are modelled as uniform slices of a cylinder (figure 1*d*). We assume that on the timescale of AP, cell rearrangements, if any, (e.g. convergent extension) can be neglected. One study [28] measured the dimensions of the basal surface of embryonic airway epithelia and noted an aspect ratio of 1.5 ± 0.3 with a surface area of $30 \pm 10\ \mu m^2$, suggesting average basal cell dimensions of approximately $5 \times 7\ \mu m$. Cell dimensions were also estimated from microscopy in a variety of developmental stages (table 1).

2.4. Subcellular model

We also analyse how tissue-scale deformations translate at a finer scale to cellular deformations and stresses, using a cell-level mechanical model, which includes some basic subcellular details. For the subcellular stress analysis, we model cells in two dimensions, corresponding visually to transverse or longitudinal cross-sections of stalk or tip. Cells are modelled as incompressible, elastic, under large plane strain, with uniform isotropic stiffness; in simulations, the nucleus is assumed to be three times as stiff as the cytoplasm but it can be many times stiffer [32]. The epithelial layer is given a uniform basal boundary displacement, compressing or stretching it.

The subcellular model was implemented in a finite-element (FEM) package, COMSOL. Numerical convergence required approximating Poisson's ratio as 0.45. For compression, the free apical surfaces were computationally defined as contact surfaces to prevent penetration of nearby boundaries. The contact problem in COMSOL involves adding a penalty function for distance, and is solved using an augmented Lagrangian method. For expansion, to ensure computational convergence at a geometric singularity, the apical cell–cell junction was given a small-radius rounding and a very fine mesh.

Table 1. Parameter estimates.

parameter	range	units	source of estimate
lumen diameter	15–50	μm	microscopy
epithelial thickness (cell height)	10–20	μm	microscopy
cell widths	3–10	μm	microscopy, [28, supplementary information]
nuclear diameter	3–6	μm	microscopy
tissue stiffness	100–200	Pa	[29–31]
cytoplasm stiffness	100–200	Pa	based on tissue stiffness
nuclear stiffness	300–2000	Pa	broad reported range; observation that nucleus generally stiffer than cytoplasm [32]

3. Results

3.1. Geometry of cell packing in a simple epithelium

In order to understand distortions of cell shape, we first need to understand the cells' initial shapes. A simple epithelium can be defined as comprising a single layer of cells bridging the space between the basal lamina and lumen. The local geometry of an epithelium determines the aspect ratios of the cells in it, and the aspect ratios of the cells' faces. Conversely, the geometry of the cells packed in an epithelium determines the overall shape of the epithelium, and ultimately its function.

Although individual cells in an epithelium can have quite different shapes and dimensions from their neighbours, notably due to differentiation and point in the cell cycle, it is useful to consider an 'average cell shape' in a regularly packed arrangement. The average cell in a simple epithelium has six neighbours, each with two hexagonal faces (apical and basal) and six trapezoidal faces (lateral) (figure 2*a*,*c*,*e*,*h*). Some epithelia have a more pronounced hexagonal packing than others, which may be a biological response to physical stress [33]. For purposes of geometric analysis, in the interest of simplicity, we also model the cells' packing in a simple epithelium as a rectangular, rather than hexagonal, grid (figure 2*b*,*d*).

Regardless of any issues of hexagonal versus rectangular packing, we can make several generalities about the average aspect ratios of the cells in a simple epithelium. Simple epithelia are classified as squamous, cuboidal or columnar; this classification is determined by the average aspect ratios of the cells' *lateral* sides. Note that the proportions of a cell change dynamically during peristalsis: a cuboidal stalk cell may be transiently compressed by peristalsis into a columnar cell, and a cuboidal tip cell may be transiently stretched into a squamous cell. Dynamic changes in aspect ratio will be discussed in greater detail later.

The *local curvature* of the epithelium determines a large number of other details of cell geometry, and vice versa:

— If the epithelium is flat, we say it has *zero curvature*. The apical and basal faces will be the same size and shape. The lateral faces will be rectangular rather than trapezoidal (figure 2*b*).
— An epithelial monolayer spheroid, or the round tip of a tubule or evagination, has a *positive curvature*, so its cells will have larger basal faces than apical faces. The lateral faces will be trapezoidal, not rectangular (figure 2*c*). The ratio of basal to apical areas and the angle of the trapezoidal lateral faces depend on cell height relative to the tissue's radius of curvature, i.e. how large the lumen is relative to the tissue thickness or cell height (figure 2*c*). Smaller monolayer spheroids have more asymmetric cell shape.
— A straight epithelial tubule has *two different curvatures*: zero curvature in the longitudinal direction and positive curvature in the circumferential direction (figures 1*b*,*c* and 2*a*,*d*). For conceptual simplicity (figure 2*d*), we can think of an average cell having four nearest neighbours, four lateral faces and two rectangular ends. The lateral faces seen in longitudinal section are rectangular, as in a flat sheet, but the lateral faces seen in transverse section are trapezoidal, as in a spheroid. As in the spheroid, the basal ends are larger than the apical ends, but they will not have the same shape: If the basal end has squarish aspect ratio (asp ~ 1), the apical end will be elongated longitudinally (asp < 1). If the apical end is squarish (asp ~ 1), then the basal end will be elongated circumferentially (asp > 1). This geometric result is independent of apicobasal surface shape: the same observation that we make for rectangular-packed cells (figure 2*d*) is true for hexagonally packed cells (figure 2*a*,*e*). We can conclude (figure 2*a*) that if the apical end is ringed by actin cables under tension, and is round, that will force the basal end, on average, to be elongated circumferentially. Conversely, if the basal end is kept round by a nearby stiff nucleus, that will force the apical end, on average, to be elongated longitudinally.
— A bent epithelial tubule also has two distinct curvatures, but on the bend's 'donut hole' side, one curvature is positive and the other negative (figure 2*f*). This is also the case at a branch point (figure 2*g*): at a branch point, cells' lateral sides will be trapezoidal; the basal and apical ends will have orientations perpendicular to each other (figure 2*h*).

3.2. Distal expansion from complete occlusion

As the tissue begins at the lumen surface, and the lumen begins at the tissue surface, we estimate the *tissue* stretches in CO by modelling distortions of the *lumen* shape. We use the simple geometry of cylinders and spheres (figure 3), accounting for conservation of lumen volume. Cell distortions then duplicate local tissue distortions, to first approximation. For an unbranched uniform tube completely occluding from its proximal end for a fraction ϵ of its length, the distal diameter will increase by a ratio $(1-\epsilon)^{-1/2}$, up to the limiting case when the tip becomes spherical (figure 3*a*–*c*). Cells adjacent to the lumen will be stretched on their apical ends in the circumferential direction by that diameter ratio; the basal ends will be stretched less. Once

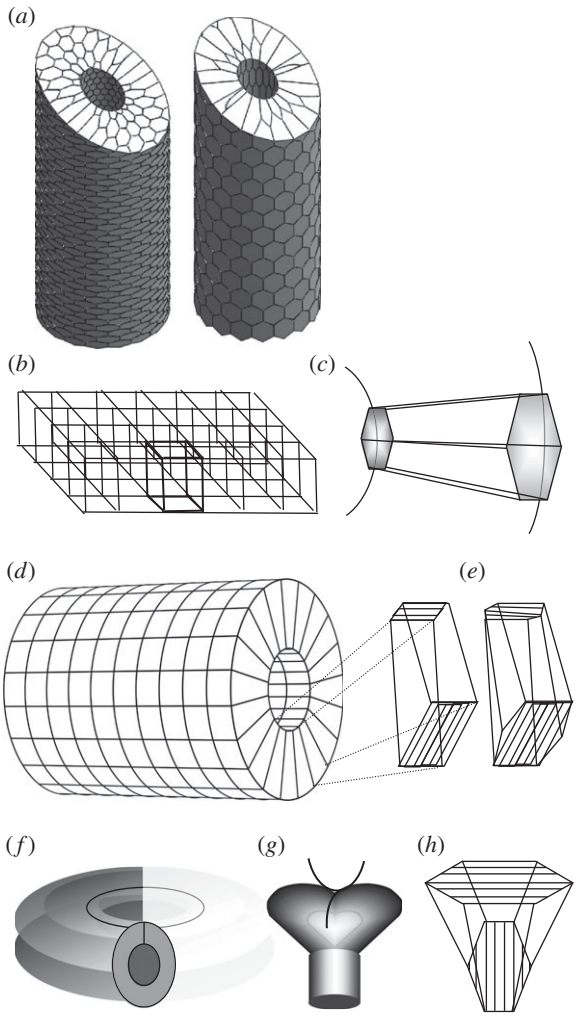

Figure 2. Geometric model of packing of 'average' cells in a simple epithelial tubule. (*a*) Real epithelia pack cells close to hexagonally, but hexagonal shapes are harder for us to analyse. (*b*) Rectangular packing is an abstraction for ease of analysis and interpretation. In a flat epithelium, apical and basal faces have the same size and aspect ratio. (*c*) Tip cells, if idealized as columnar, have the same aspect ratios on apical and basal faces, but the basal face is always larger than the apical face. This is a simple consequence of the geometry. (*d*) Idealized cell shape in square-packed tubule is curved on apical and basal sides. There are two distinct lateral face shapes: wedge-shaped on two faces, and rectangular on the other two. Basal and apical faces are oriented in perpendicular directions: basal surfaces are elongated circumferentially, while apical surfaces are elongated longitudinally. This is a simple consequence of the geometry. (*e*) In a hexagonally packed stalk as in (*a*), the basal face will be more circumferentially oriented than the apical face, just as in (*d*). Sheets (*b*) have zero curvature; spheroids and round tips (*c*) have positive curvature in all directions; tubules (*d*) have positive curvature in the transverse direction and zero curvature longitudinally; curved tubules (*f*) and branch points (*g*) have places where the curvature is positive in one direction and negative in the other. Those locations have cells whose apical and basal faces have perpendicular orientations (*h*).

the occlusion has propagated close enough to the tip to inflate it to a sphere, we can estimate the increase in diameter of the tip: if a length L (in tube diameters) of stalk fluid has inflated the tip, the tip's diameter has increased by a ratio of $(1 + 1.5L)^{1/3}$ (figure 3*d*,*e*). We have observed *in vitro* pseudoglandular embryonic airway tips expanding approximately double in diameter due to AP [34]. That amount of expansion would be accomplished by propagating a CO a length of $14/3 \sim 5$ diameters to the tip.

3.3. Geometry of epithelial stretching

Each cell in a tissue is subject to different stretches in the three directions (figure 1*c*,*d*). Cell distortion (strain) consists of lengthening or shortening in each of three directions: apicobasal (radial), proximodistal (longitudinal) and circumferential (hoop). Additionally, there is some shear (skew) distortion. However, if the tube and occlusion are radially symmetric, there is only one possible shear mode (figure 1*c*). Conservation of cell volume on the timescale of peristalsis requires that lengthening in one or two directions is balanced by shortening in the other (figure 4).

The geometry of a uniform tube with a closed, rounded tip implies several results, regardless of mechanical aspects such as tissue stiffness, and regardless of how cells are packed between their neighbours. First, because cells do not change their volume during transient peristalsis, if a cell is stretched in one dimension, it must be compressed in another dimension (figure 1*b*). If AP stretches an airway tip, the tip cells' apical and basal areas increase, so its apicobasal height must decrease a corresponding amount, and that amount can be substantial (figures 1*b* and 4*a*). At a peristaltic stenosis, when the apical end of a cell is compressed to almost nothing, even though the tubule diameter is reduced, the epithelial cells in that compressed region must elongate in the apicobasal direction, and that elongation may be substantial (figure 4*b*).

In a straight tubular geometry, although an epithelial cell's apical surface is smaller than its basal surface, both stretch and compression (ratios) will always be greater at the apical surface than at the basal surface. For example, doubling the internal diameter of a branch tip (figure 4*a*) doubles the apical cell diameter and quadruples apical surface area, but stretches a cell's basal surface by a much smaller proportion. Similarly, CO (figure 4*b*) compresses the local basal surface a certain percentage, but compresses the local apical surface to zero area. These effects are modulated by lumen diameter: for a given epithelial thickness, the smaller the relaxed lumen diameter, the more pronounced is the difference in stretch ratios between the apical and basal ends of epithelial cells (figure 4, black and white bars), because the tissue curvature is greater.

At the tip, because of symmetry, conservation of cell volume mandates that apicobasal compression is exactly double the surface stretch (figure 4*b*). More interesting, perhaps, is that at the tip, circumferential (hoop) stretch and longitudinal stretch become identical, because the tip is locally spherical. A stalk cell is both shaped differently and stretched differently in the circumferential and longitudinal directions, but a cell at the tip would not be able to detect, from its shape or its stretch, which direction is circumferential and which is longitudinal.

3.4. Intracellular stretch and stress

Averaging spatially across several cells, the stresses on whole cells and their corresponding strains (or stretches) correspond to the stresses and strains of the tissue they make up. At a finer level, however, there are important *localized* stress concentrations at specific locations in the cell. Therefore, we developed a model of the subcellular stresses and stretches when a simple epithelium is deformed by peristalsis.

While the basal surface is bound to ECM, constraining its shape, the apical surface is free to change its shape.

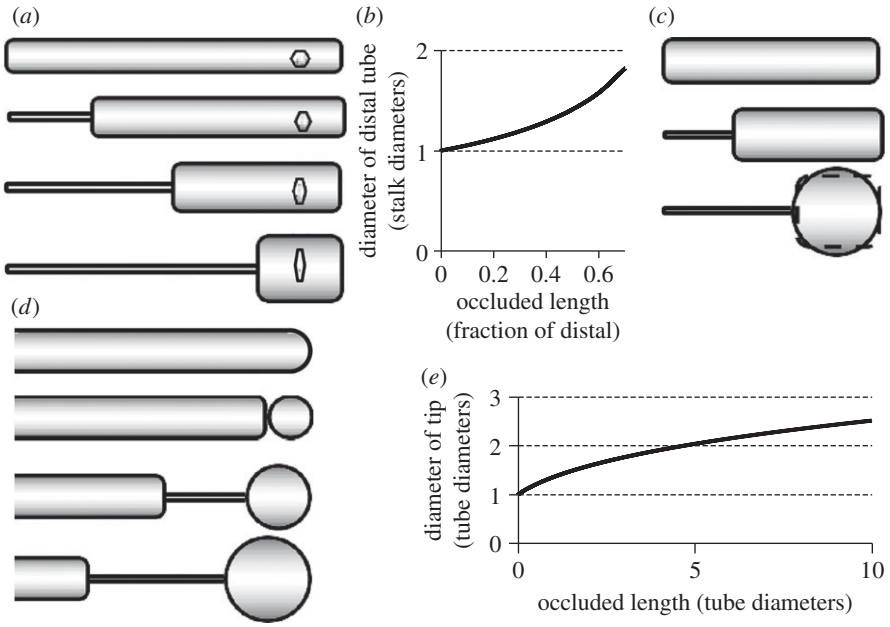

Figure 3. Conservation of lumen fluid determines cell stretches. In complete occlusion, distal tissues stretch to accommodate lumen volume from elsewhere. Geometric analysis quantifies tissue distortions. Panels (*a*), (*c*) and (*d*) show shape of lumen as complete occlusion moves distally. (*a*,*b*) For occlusion far from tip, distal stalk remains approximately cylindrical, and lumen diameter (and therefore lumen circumference) increase as $(1 - \epsilon)^{-1/2}$, where ϵ is the proportion of the length that has been completely occluded. Assuming that cells are not rearranged by tissue stretches, the stretch of apical ends of cells must exactly match the stretch of the lumen surface. (*c*). If volume is pushed far enough distally, the tip region will become spherical. In the immediate region of the tip, we model the pressurized lumen as a sphere. (*d*,*e*) Inflated tip lumen diameter increases as $(1 + 1.5L)^{1/3}$ where L is the length (in tube diameters) of occluded region. All lumen deformations drawn to scale.

Thus, the apical end is under less stress than the rest of the cell. However, the geometry of the free apical surface concentrates stresses at the apical cell–cell junctions (figure 5), both in compression and in tension. This induces a tugging on cell–cell contacts, which has been shown to regulate the junctions themselves [35]. Because the free apical surface changes shape, there is a small shear stress (and strain) near the apical cell–cell junctions; elsewhere, there is negligible shear.

Deformation of the tissue and its cells also deforms the nuclei. Nuclei are generally stiffer than the cytoplasm [36]. This causes localized stress gradients due to the stiffness mismatch, both in compression and in tension (figure 5). If nuclei of adjacent cells are aligned, there will be a band of stress concentration between nuclei (figure 5).

4. Discussion

It has been proposed [22] that prenatal AP may play a role in the development of the lung, because disruption of AP leads to hypoplastic lung development [14]. If we look for intermediate mechanisms of this influence, we make several broad hypotheses: (i) long-distance transport of morphogens [11], (ii) flow sensing [11,12], and (iii) stretch sensing. We cannot correctly interpret the experiments without untangling these three potentially coupled intermediate mechanisms both with models and with additional more targeted experiments. The first two intermediate mechanisms are addressed in two papers [11,12], which develop a quantitative framework for hypothetical flow sensing and morphogen transport in the context of AP. This paper provides an analytical basis for interpreting potential mechanisms of the morphogenetic influence of AP through stretch sensing.

The most striking results of this paper come from a very simple geometric analysis. We point out that when a tubule is completely occluded by a peristaltic contraction, or when a distal tip is inflated by peristalsis-pumped proximal fluid, the stretches can be enormous, changing the aspect ratio, or surface area, or length, by double or more. Stretches that large can have the effect of fluidizing the cytoskeleton [37]; even much smaller stretches should have a large effect on cell signalling, through breaking of adhesions, opening of channels, straightening of coiled polymers and alignment of randomly oriented polymers. As dramatic as these cell stretches are, they have hardly been considered at all in the development of the lung, even though we would not expect a cell to physiologically or developmentally ignore being cyclically stretched or squashed. We note that our analysis of the cell shape changes should hold regardless of the source of the occlusion, e.g. peristalsis or tonic SM contractions [21].

A cell can only directly sense its immediate environment, yet our geometric analysis suggests that this local information could potentially provide a cell with a kind of positional information. Stretch is a change in length relative to some initial length. Thus, for a cell to sense its stretch, it must first have some sense of its baseline geometry. Can a cell tell what shape it is? If so, can it tell where it is? Cell shape strongly influences division orientation [38] and thereby morphogenesis [39]. Cell shape has been shown to determine cell fate (reviewed in [40]), in part through regulating nuclear shape [41] via a linkage through the perinuclear cytoskeleton [42]. By examining how cells pack in a simple epithelium, our results (figure 2) can explain how a cell might infer positional information, as well as orientational and other anatomical information: cells packed close to uniformly in an epithelium have locally average shapes characteristic of the local curvature of the epithelium. The

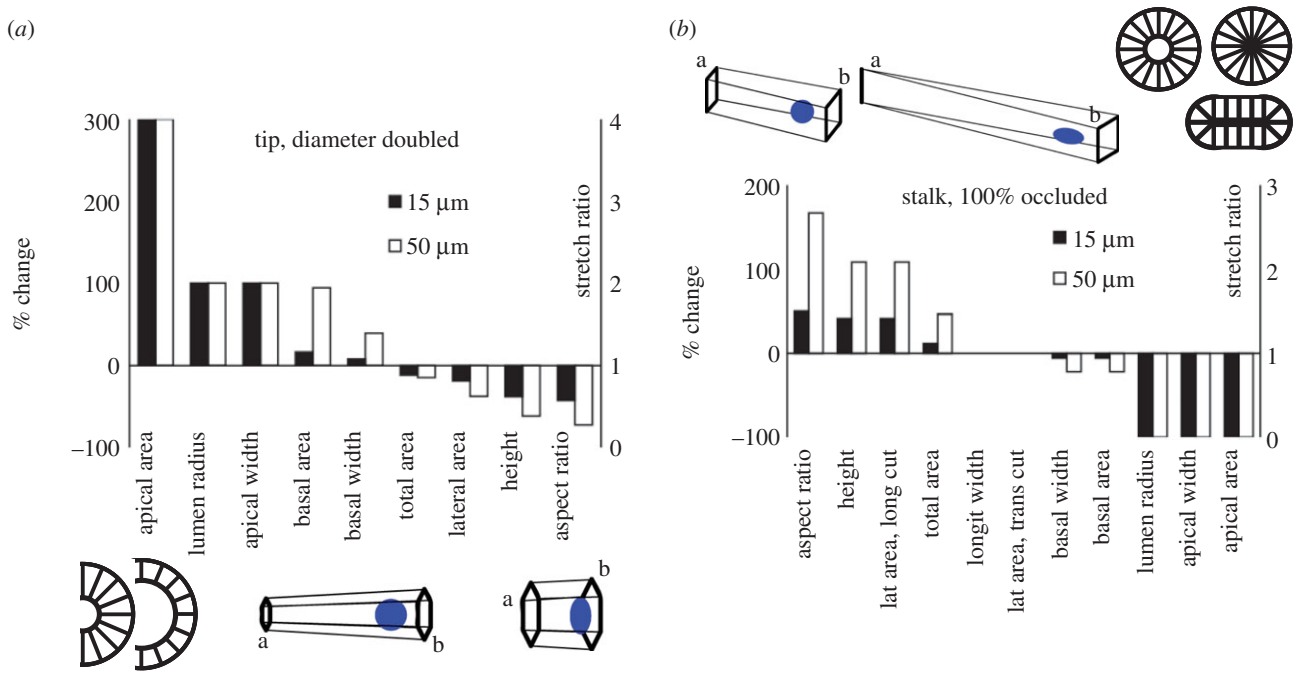

Figure 4. Peristalsis-induced tissue distortion distorts individual cells proportionally. Tissue deformations impose different deformations on specific cell parts. Cell dimensional changes (% of relaxed dimensions, ratio of deformed to initial dimensions) depend in part on initial geometry. Shown are deformations of cells in a simple epithelium with relaxed epithelial thickness of 15 µm, and initial lumen diameter of 15 or 50 µm. Results will be similar for different baseline dimensions. (*a*) Stretches of tip cells. Any peristaltic pulse which doubles tip lumen diameter must double the tip cells' apical width and quadruple the tip cells' apical area, while substantially flattening cells. All tip cell dimensions except apical width and area are affected more strongly by lumen doubling when lumen diameter is initially larger (50 versus 15 µm). (*b*) Stretches of stalk cells. Complete occlusion pinches stalk cells' apical ends to zero width and zero area, while dramatically increasing cell height and aspect ratio. The stalk cells' total area is increased, primarily on the lateral surfaces. The height, aspect ratio and total surface area are changed more if the lumen was initially larger (50 versus 15 µm diameter). It is unknown whether complete occlusion is symmetric like segments of an orange, or if tissue stiffness resists deformation, causing buckling (ovaling) like a pinched hose. (*a,b*). In every case, apical, a, % distortions (strains) are greater than basal, b, distortions. Nuclear stretch is exaggerated in illustration; nuclei are generally stiffer than whole cells, so nuclear deformation will be smaller than nearby cytoplasmic deformation (figure 5). (Online version in colour.)

local curvature is what geometrically distinguishes a tubule from a tip or a cleft.

A static cell in a simple epithelium would obviously be able to tell which of its ends was apical and which basal, but determining where it is located in a tubule is less obvious. But a cell could, in theory, tell if it was most probably residing in a tip or a stalk or a cleft based on the local curvature of the epithelium, solely by knowing its own dimensions (perhaps, e.g., by gauging microtubule length), on the assumption that its neighbours are of approximately the same dimensions. A tip is convex in both directions, which means that a tip cell's basal dimensions are both greater than its apical dimensions. Straight stalks are locally convex in the circumferential direction but flat in the longitudinal direction, so their cells must be of different aspect ratios on their apical and basal surfaces. A cleft (branch junction) is locally convex in one direction and concave in the other direction, so its epithelial cells on average have perpendicular orientations on their apical and basal ends. By the same geometric principles, a cell in a simple epithelium could also (in theory) detect the local tubule diameter, by comparing the ratio of its basal and apical ends, and its apicobasal length.

Morphogenetic mechanisms based on cell stretch would naturally depend on the location of the stretch. We analysed the deformations of epithelial cells in the stalk adjacent to SM contraction and in the tip of a tubule distended by AP (figures 3 and 4). Owing to geometry alone, the largest stretches and compressions are on the apical end of a cell. Cells stretched in one direction are compressed in another direction, and their aspect ratios can change dramatically in response to AP. These dramatic dynamic changes in aspect ratios of the cell volume and surfaces, also known as anisotropic strain, could function as a stress probe helping to organize cell packing in the epithelium [33]. A partial analogy can be seen in a box of long-grained rice: vibrating the box causes the rice to pack into a smaller volume, because it provides the opportunity for adjacent grains to align, which increases the packing efficiency. Another partial analogy is seen in a sweater suffering a short snagged loop: stretching the fabric a few times pulls the loop back in, restoring the geometric equilibrium of the knit.

While doubling or halving a length in a tissue corresponds to doubling or halving lengths in cells, specific locations in a cell will experience different stresses. Our model of subcellular stresses shows that while most stress is uniform, there are stress concentrations in the vicinity of the nucleus, and substantial stress concentrations at the apical cell–cell junction. We suggest that the large cyclic strains of AP may serve to rearrange cells and stimulate other mechanosensitive processes by repeatedly breaking and reforming lateral cell–cell adhesions. We further suggest that stress concentrations between nuclei of adjacent cells may serve as a signal guiding alignment of nuclei as an epithelium matures, in a process similar to the stress probing described above.

This paper presented a suite of models of geometry, volume conservation and elastic deformation of epithelia and their cells in embryonic AP. The models follow the

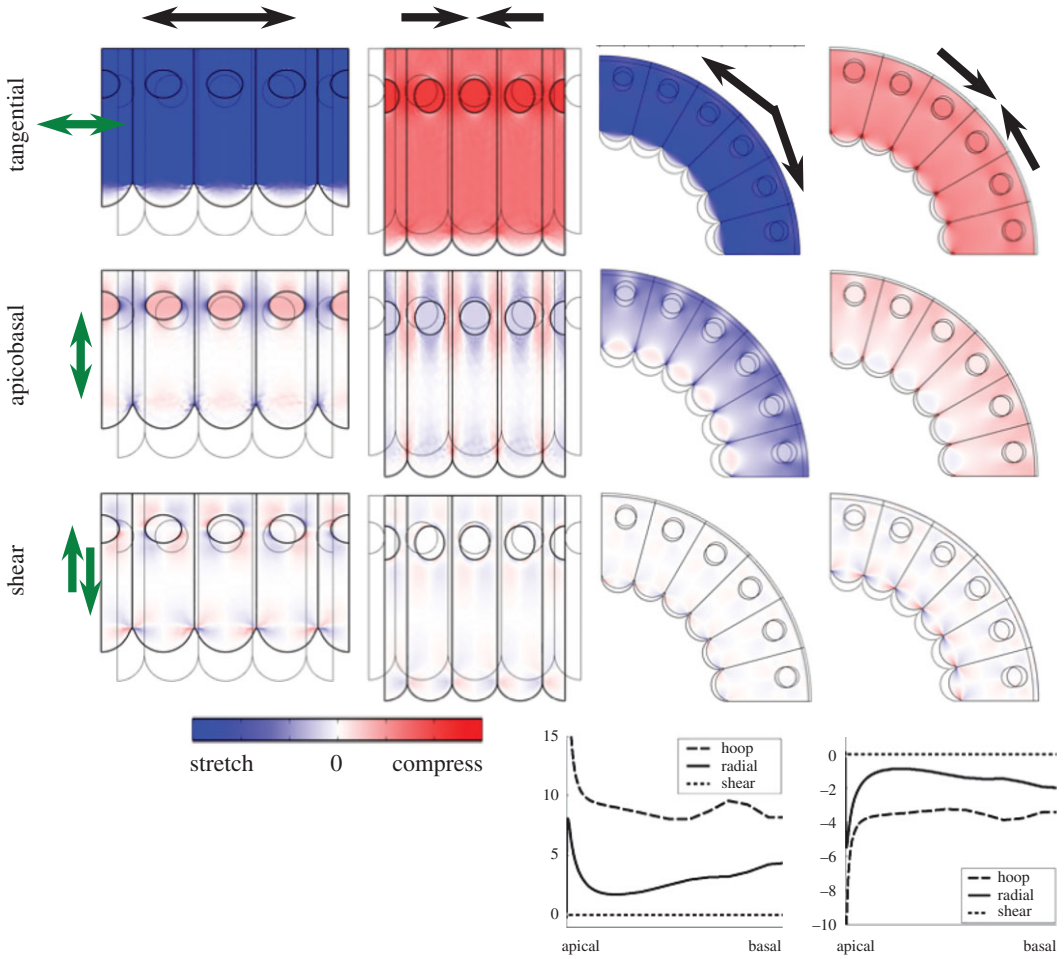

Figure 5. Two-dimensional model of epithelial tubule as seen in longitudinal (left two columns) and transverse (right two columns) slices. The basal surface is bound to the basal lamina; the apical surface is free. Nuclei are three times stiffer than cytoplasm. Colour shows stress magnitude. Graphs (bottom row) show stress magnitudes in transverse slice along the entire cell–cell boundary, in compression and tension. Stress perpendicular to cell–cell junctions (tangential, hoop) is roughly double the apicobasal (radial) stress. Compression and tension of epithelium create notable hoop (tangential) stress concentrations near nuclei and high hoop and radial stress at apical cell–cell junctions.

principle of parsimony—maximizing the ratio of insight to complexity. Clearly, many of the assumptions built into them are simpler than observed reality, and once we have understood the simpler foundational models completely, we can examine where they deviate from the natural system that they model, and whether the differences in inputs and outputs are significant. Within this paper, we compare results of a simpler model which assumes uniform material properties everywhere (figure 4) with results of a more detailed/realistic model which reveals additional phenomena such as localized stress concentrations (figure 5). The comparison of different models' assumptions and results highlights which system features (e.g. a stiffer nucleus) are associated with which emergent behaviour (e.g. stress concentrations).

Some model simplifying assumptions are biologically insignificant. For example, for algebraic simplicity, we used the approximation of no longitudinal strain. Making the model mechanically more precise by including the longitudinal strain would yield an insignificant improvement in accuracy, compared with much more substantial simplifying assumptions such as uniform material properties and a symmetrically occluded lumen.

Some model simplifying assumptions may have some biological significance worth examining. For example, this paper assumed identical cells everywhere in the epithelium. Yet clearly, e.g., dividing cells are not the same shapes as non-dividing neighbour cells. Even among cells at the same stage in the cell cycle and the same general position in the tissue, there will be some morphological variation, e.g. in a pseudo-stratified epithelium, where the cells' lateral surfaces are not strictly perpendicular to the epithelial surface. Could local variation in cell shape potentially be a source of randomness determining local differentiation? Our analysis of epithelial curvature and its relationship to cell shape could potentially indicate positional information guiding oriented cell divisions [28] and the differentiation of airway epithelial tissues [43]. Our models in this paper also assumed complete conservation of volume of lumen fluid. In our previous papers [11,12], we analysed flows of lumen fluid through and proximal to the stenosis. But it is theoretically possible that peristaltic lumen pressure sufficient to distend the epithelial tip by a large amount is also sufficient to drive fluid distally through gaps in the pericellular space to the interstitium, which would certainly be biologically significant.

While this paper focused on epithelia, there are other tissues in the developing lung which are also mechanically responsive. Airway SM (ASM) is known to be sensitive to strain, increasing both differentiation and production of myosin and MLCK [44]; AP in the embryo may also serve to stimulate ASM differentiation and hypertrophy.

While this paper focuses specifically on the subtype of mechanotransduction classified as stretch sensing, there are of course other subtypes. A previous paper [11] discusses issues related to flow sensing and makes specific predictions as to the likely nature of flow-sensing mechanisms in the embryonic lung epithelium. This paper ignores flow sensing, and also ignores all tissues but the epithelium. It seems likely that there are multiple mechanisms of mechanotransduction operating in the embryonic lung, simultaneously, and that they affect each other, at least indirectly, but possibly directly (through mechanical coupling between cell components). It is not the goal of this paper to declare a comprehensive understanding of the interactions of all cell components, known and unknown. Rather, we aim to provide specific stretch and stress estimates relevant to the context of AP, as a guide to refining hypotheses and designing and interpreting experiments, which may ultimately lead to an improved understanding of mechanotransduction and morphogenesis in the embryonic airway.

Competing interests. We declare we have no competing interests.

Funding. This work was supported in part by NIH R01 GM096195 to S.R.L. S.R.L. would also like to thank the Isaac Newton Institute for Mathematical Sciences for its hospitality during the programme 'Coupling geometric PDEs with physics for cell morphology, motility and pattern formation' supported by EPSRC grant no. EP/K032208/1 and a fellowship from the Simons Foundation.

References

1. Xavier-Neto J, Castro R, Sampaio A, Azambuja A, Castillo H, Cravo R, Simoes-Costa M. 2007 Cardiovascular development: towards biomedical applicability: parallel avenues in the evolution of hearts and pumping organs. *Cell. Mol. Life Sci.* **64**, 719–734. (doi:10.1007/s00018-007-6524-1)
2. Fung YC, Yih CS. 1968 Peristaltic transport. *J. Appl. Mech.* **35**, 669–675. (doi:10.1115/1.3601290)
3. Shapiro AH, Jaffrin MY, Weinberg SL. 1969 Peristaltic pumping with long wavelengths at low Reynolds number. *J. Fluid Mech.* **37**, 799–825. (doi:10.1017/S0022112069000899)
4. Jaffrin MY, Shapiro AH. 1971 Peristaltic pumping. *Annu. Rev. Fluid Mech.* **3**, 13–37. (doi:10.1146/annurev.fl.03.010171.000305)
5. Burns JC, Parkes T. 1967 Peristaltic motion. *J. Fluid Mech.* **29**, 731–743. (doi:10.1017/S0022112067001156)
6. Yin F, Fung Y. 1971 Comparison of theory and experiment in peristaltic transport. *J. Fluid Mech.* **47**, 93–112. (doi:10.1017/S0022112071000958)
7. Pozrikidis C. 1987 A study of peristaltic flow. *J. Fluid Mech.* **180**, 515–527. (doi:10.1017/S0022112087001939)
8. Grotberg JB, Jensen OE. 2004 Biofluid mechanics in flexible tubes. *Annu. Rev. Fluid Mech.* **36**, 121–147. (doi:10.1146/annurev.fluid.36.050802.121918).
9. Takabatake S, Ayukawa K, Mori A. 1988 Peristaltic pumping in circular cylindrical tubes: a numerical study of fluid transport and its efficiency. *J. Fluid Mech.* **193**, 267–283. (doi:10.1017/S0022112088002149)
10. Aranda V, Cortez R, Fauci L. 2011 Stokesian peristaltic pumping in a three-dimensional tube with a phase-shifted asymmetry. *Phys. Fluids* **23**, 081901. (doi:10.1063/1.3622319)
11. Bokka KK, Jesudason EC, Lozoya OA, Guilak F, Warburton D, Lubkin SR. 2015 Morphogenetic implications of peristalsis-driven fluid flow in the embryonic lung. *PLoS ONE* **10**, e0132015. (doi:10.1371/journal.pone.0132015)
12. Bokka KK, Jesudason EC, Warburton D, Lubkin SR. 2015 Morphogenetic implications of peristaltic fluid–tissue dynamics in the embryonic lung. *J. Theor. Biol.* **382**, 378–385. (doi:10.1016/j.jtbi.2015.06.022)
13. Schittny JC, Miserocchi G, Sparrow MP. 2000 Spontaneous peristaltic airway contractions propel lung liquid through the bronchial tree of intact and fetal lung explants. *Am. J. Respir. Cell Mol. Biol.* **23**, 11–18. (doi:10.1165/ajrcmb.23.1.3926)
14. Jesudason EC, Smith NP, Connell MG, Spiller DG, White MR, Fernig DG, Losty PD. 2005 Developing rat lung has a sided pacemaker region for morphogenesis-related airway peristalsis. *Am. J. Respir. Cell Mol. Biol.* **32**, 118–127. (doi:10.1165/rcmb.2004-0304OC)
15. Parvez O, Voss AM, de Kok M, Roth-Kleiner M, Belik J. 2006 Bronchial muscle peristaltic activity in the fetal rat. *Pediatr. Res.* **59**, 756–761. (doi:10.1203/01.pdr.0000219121.15634.d1)
16. Pandya HC, Innes J, Hodge R, Bustani P, Silverman M, Kotecha S. 2006 Spontaneous contraction of pseudoglandular-stage human airspaces is associated with the presence of smooth muscle-alpha-actin and smooth muscle-specific myosin heavy chain in recently differentiated fetal human airway smooth muscle. *Biol. Neonate* **89**, 211–219. (doi:10.1159/000089797)
17. Heisenberg C-P, Bellaïche Y. 2013 Forces in tissue morphogenesis and patterning. *Cell* **153**, 948–962. (doi:10.1016/j.cell.2013.05.008)
18. Liu M, Post M. 2000 Invited review: mechanochemical signal transduction in the fetal lung. *J. Appl. Physiol.* **89**, 2078–2084.
19. Tschumperlin DJ, Boudreault F, Liu F. 2010 Recent advances and new opportunities in lung mechanobiology. *J. Biomech.* **43**, 99–107. (doi:10.1016/j.jbiomech.2009.09.015)
20. Adzick NS, Harrison MR, Glick PL, Villa RL, Finkbeiner W. 1984 Experimental pulmonary hypoplasia and oligohydramnios: relative contributions of lung fluid and fetal breathing movements. *J. Pediatr. Surg.* **19**, 658–665. (doi:10.1016/S0022-3468(84)80349-8)
21. McCray PB. 1993 Spontaneous contractility of human fetal airway smooth muscle. *Am. J. Respir. Cell Mol. Biol.* **8**, 573–580. (doi:10.1165/ajrcmb/8.5.573).
22. Jesudason EC. 2009 Airway smooth muscle: an architect of the lung? *Thorax* **64**, 541–545. (doi:10.1136/thx.2008.107094)
23. Warburton D, Olver B. 1997 Coordination of genetic, epigenetic, and environmental factors in lung development, injury, and repair. *Chest* **111**, 119S–122S. (doi:10.1378/chest.111.6_Supplement.119S)
24. Jesudason EC. 2006 Small lungs and suspect smooth muscle: congenital diaphragmatic hernia and the smooth muscle hypothesis. *J. Pediatr. Surg.* **41**, 431–435. (doi:10.1016/j.jpedsurg.2005.11.021)
25. Unbekandt M, del Moral PM, Sala FG, Bellusci S, Warburton D, Fleury V. 2008 Tracheal occlusion increases the rate of epithelial branching of embryonic mouse lung via the FGF10-FGFR2b-Sprouty2 pathway. *Mech. Dev.* **125**, 314–324. (doi:10.1016/j.mod.2007.10.013)
26. George UZ, Bokka KK, Warburton D, Lubkin SR. 2015 Quantifying stretch and secretion in the embryonic lung: implications for morphogenesis. *Mech. Dev.* **138**, 356–363. (doi:10.1016/j.mod.2015.07.003)
27. Swift J *et al.* 2013 Nuclear lamin-A scales with tissue stiffness and enhances matrix-directed differentiation. *Science* **341**, 1240104. (doi:10.1126/science.1240104)
28. Tang N, Marshall WF, McMahon M, Metzger RJ, Martin GR. 2011 Control of mitotic spindle angle by the RAS-regulated ERK1/2 pathway determines lung tube shape. *Science* **333**, 342–345. (doi:10.1126/science.1204831)
29. Alcaraz J, Buscemi L, Grabulosa M, Trepat X, Fabry B, Farré R, Navajas D. 2003 Microrheology of human lung epithelial cells measured by atomic force microscopy. *Biophys. J.* **84**, 2071–2079. (doi:10.1016/S0006-3495(03)75014-0)
30. Wiebe C, Brodland GW. 2005 Tensile properties of embryonic epithelia measured using a novel instrument. *J. Biomech.* **38**, 2087–2094. (doi:10.1016/j.jbiomech.2004.09.005)
31. Fabry B, Maksym GN, Butler JP, Glogauer M, Navajas D, Taback NA, Millet EJ, Fredberg JJ. 2003 Time scale and other invariants of integrative mechanical behavior in living cells. *Phys. Rev. E* **68**, 41914. (doi:10.1103/PhysRevE.68.041914)
32. Dahl KN, Ribeiro AJ, Lammerding J. 2008 Nuclear shape, mechanics, and mechanotransduction. *Circ. Res.* **102**, 1307–1318. (doi:10.1161/CIRCRESAHA.108.173989)

33. Sugimura K, Ishihara S. 2013 The mechanical anisotropy in a tissue promotes ordering in hexagonal cell packing. *Development* **140**, 4091–4101. (doi:10.1242/dev.094060)
34. Warburton D *et al.* 2010 Chapter three-lung organogenesis. *Curr. Top. Dev. Biol.* **90**, 73–158. (doi:10.1016/S0070-2153(10)90003-3)
35. Liu Z, Tan JL, Cohen DM, Yang MT, Sniadecki NJ, Ruiz SA, Nelson CM, Chen CS. 2010 Mechanical tugging force regulates the size of cell-cell junctions. *Proc. Natl Acad. Sci. USA* **107**, 9944–9949. (doi:10.1073/pnas.0914547107)
36. Lammerding J, Dahl KN, Discher DE, Kamm RD. 2007 Nuclear mechanics and methods. *Methods Cell Biol.* **83**, 269–294. (doi:10.1016/S0091-679X(07)83011-1)
37. Trepat X, Deng L, An SS, Navajas D, Tschumperlin DJ, Gerthoffer WT, Butler JP, Fredberg JJ. 2007 Universal physical responses to stretch in the living cell. *Nature* **447**, 592–595. (doi:10.1038/nature05824)
38. Théry M, Bornens M. 2006 Cell shape and cell division. *Curr. Opin Cell Biol.* **18**, 648–657. (doi:10.1016/j.ceb.2006.10.001)
39. Xiong F *et al.* 2014 Interplay of cell shape and division orientation promotes robust morphogenesis of developing epithelia. *Cell* **159**, 415–427. (doi:10.1016/j.cell.2014.09.007)
40. Sun Y, Chen CS, Fu J. 2012 Forcing stem cells to behave: a biophysical perspective of the cellular microenvironment. *Annu. Rev. Biophys.* **41**, 519–542. (doi:10.1146/annurev-biophys-042910-155306)
41. Versaevel M, Grevesse T, Gabriele S. 2012 Spatial coordination between cell and nuclear shape within micropatterned endothelial cells. *Nat. Commun.* **3**, 671. (doi:10.1038/ncomms1668)
42. Lozoya OA, Gilchrist CL, Guilak F. 2016 Universally conserved relationships between nuclear shape and cytoplasmic mechanical properties in human stem cells. *Sci. Rep.* **6**, 23047. (doi:10.1038/srep23047)
43. Rawlins EL. 2008 Lung epithelial progenitor cells: lessons from development. *Proc. Am. Thorac. Soc.* **5**, 675–681.
44. Smith PG, Moreno R, Ikebe M. 1997 Strain increases airway smooth muscle contractile and cytoskeletal proteins *in vitro*. *Am. J. Physiol. Lung Cell. Mol. Physiol.* **272**, L20–L27.